Nuclear Inst. and Methods in Physics Research, A 1032 (2022) 166527

Contents lists available at ScienceDirect

Nuclear Inst. and Methods in Physics Research, A

journal homepage: www.elsevier.com/locate/nima

Characterization of mixed $Bi_4(Ge_xSi_{1-x})_3O_{12}$ for crystal calorimetry at future colliders

R. Cala' [a,b,*], N. Kratochwil [a,c], L. Martinazzoli [a,b], M.T. Lucchini [b], S. Gundacker [d], E. Galenin [e], I. Gerasymov [e,f], O. Sidletskiy [e,f], M. Nikl [g], E. Auffray [a]

[a] European Organization for Nuclear Research (CERN), Geneva, Switzerland
[b] INFN & Università degli Studi di Milano-Bicocca, Milan, Italy
[c] University of Vienna, Vienna, Austria
[d] PMI ExMI RWTH Aachen University, Aachen, Germany
[e] Institute for Scintillation Materials NAS of Ukraine, 60 Nauky Ave., Kharkiv, Ukraine
[f] Institute of Physics, Kazimierz Wielki University in Bydgoszcz, Bydgoszcz, Poland
[g] Institute of Physics of the Czech Academy of Sciences, Prague, Czech Republic

ARTICLE INFO

Keywords:
Mixed crystals
Dual-readout calorimetry
BGO
BSO
Cherenkov emission

ABSTRACT

Bismuth germanate (BGO) is a well known high density scintillating material widely used in many applications such as high energy physics and medical imaging. Bismuth silicate (BSO) features properties similar to BGO in terms of stopping power and Cherenkov photon yield with a lower scintillation light output but faster decay time, thus being more attractive for applications in high-rate environments. Mixed crystals such as $Bi_4(Ge_xSi_{1-x})_3O_{12}$ (BGSO, with x varying from 0 to 1) make it possible to optimize decay time and light yield based on the detector needs.

A characterization campaign of the optical and scintillation properties of two sets of BGSO mixed crystals with Ge fraction varying from 0 to 100% was performed. A coincidence time resolution (CTR) at 511 keV of 208 ±2 ps FWHM was measured for a $2 \times 2 \times 3$ mm^3 pixel with 40% Ge, while the optimum value obtained for the effective decay time is 49.9 ±1.8 ns for a $6 \times 6 \times 0.7$ mm^3 plate-shaped sample with 30% Ge. Furthermore the smallest slow decay time component achieved is 101 ±2 ns and is obtained for the plate-shaped sample with 30% Ge, while the largest is 236 ±5 ns for a pure BGO sample with the same geometry.

In addition we demonstrated the possibility to efficiently separate the Cherenkov and scintillation light produced in a pure BSO sample. Such a technique could be exploited in a crystal-based dual-readout calorimeter to improve the energy resolution for hadronic showers and jets.

1. Introduction

Scintillating crystals characterized by their high density have been largely employed in calorimetry as they are able to provide for excellent energy resolution when detecting electrons and photons [1–4]. However, they usually have a poor hadronic performance because of their large e/h ratio [5]. A renewed interest in these materials comes from recent developments in photodetector technologies [6] which open new possibilities to exploit Cherenkov emission in addition to scintillation light for dual-readout calorimetry at future collider experiments to improve the energy resolution for hadronic showers and jets [7]. A possible way to implement dual-readout calorimetry with homogeneous crystals could be the simultaneous use of two different SiPMs (one with high UV sensitivity) coupled to the same scintillator. Studies on bismuth germanate ($Bi_4Ge_3O_{12}$) have shown the possibility to separate Cherenkov radiation from scintillation emission by means of optical filters, despite the fact that Cherenkov photons represents only a small amount (~ 1%) of the light produced in this material [8,9].

BGO was widely used in particle physics experiments because of its high density, short radiation length and relatively high light output [1,2]. As a drawback, this crystal has a large decay time and moderate radiation hardness which limits its application, especially in high energy physics experiments where fast timing and high radiation hardness are required. Bismuth silicate (BSO), which has the same crystal structure as BGO with silicon atoms instead of germanium ones, seems to be a possible alternative because of its shorter decay time and better radiation hardness (~ 100 ns and $10^5 - 10^6$ rad respectively, compared

* Corresponding author at: European Organization for Nuclear Research (CERN), Geneva, Switzerland.
E-mail addresses: roberto.cala'@cern.ch (R. Cala'), nicolaus.kratochwil@cern.ch (N. Kratochwil), loris.martinazzoli@cern.ch (L. Martinazzoli), marco.toliman.lucchini@cern.ch (M.T. Lucchini), Stefan.Gundacker@cern.ch (S. Gundacker), galenin@isma.kharkov.ua (E. Galenin), gerasimov@isma.kharkov.ua (I. Gerasymov), sidletskiy@isma.kharkov.ua (O. Sidletskiy), nikl@fzu.cz (M. Nikl), Etiennette.Auffray@cern.ch (E. Auffray).

https://doi.org/10.1016/j.nima.2022.166527
Received 27 September 2021; Received in revised form 8 February 2022; Accepted 23 February 2022
Available online 18 March 2022

Table 1
Physical properties of BGO, BSO and PWO crystals. The refractive index is given at peak emission wavelength. The values in this table have been taken from [14], unless specified.

Property	BGO	BSO	PWO
Density (g cm^{-3})	7.13	7.12	8.28
Radiation length (cm)	1.12 [10]	1.15 [10]	0.89 [15]
Refractive index	2.15 [10]	2.06 [10]	2.36 [15]
Peak emission (nm)	480 [10]	480 [10]	420 [15]
Light output (photons/MeV)	8200	1200	100
Decay time (ns)	300	100	6

with ~ 300 ns and $10^4 - 10^5$ rad of BGO) [10–12]. In addition, BSO has a transmission cutoff blue-shifted with respect to BGO, which allows to exploit a wider wavelength range to extract Cherenkov radiation from such scintillator. One of the main drawbacks of BSO compared to BGO is the difficulty in growing large size crystal because of its near-congruent melting composition. However, to employ mixed crystals by partial replacement of Si by Ge in the host could be a possible solution to overcome the issue [13]. In Table 1 relevant properties of both these crystals and $PbWO_4$ (PWO) are provided [10,14,15]. Such scintillating and optical properties of BSO make it a leading candidate for applications in dual-readout calorimetry at future e^+e^- colliders.

The aim of this paper is to evaluate scintillating and timing properties of mixed BGSO materials ($Bi_4(Ge_xSi_{1-x})_3O_{12}$, with x varying from 0 to 1) and compare them with the ones obtained for pure BGO and BSO samples. The transmission spectra, light output, energy resolution, coincidence time resolution and the scintillation kinetic properties of the samples under test were characterized. The last part of the paper is focused on the possibility to separate Cherenkov and scintillation emission from a BSO bulk by means of optical filters.

2. Materials and methods

2.1. Crystal samples

In the study presented in this paper, two different sets of mixed $Bi_4(Ge_xSi_{1-x})_3O_{12}$ samples with percentage of germanium varying from 0% to 100% were characterized. The first one was produced by Shonan Institute of Technology, Fujisawa (Japan) and consists of optically polished plate-shaped samples having Ge fractions x equal to 0, 0.1, 0.3, 0.5, 0.7, 0.9 and 1, while the other set comes from the Institute for Scintillation Materials of NAS (Ukraine) and consists of bulks having different state of surface polishing and dimensions and Ge fractions x equal to 0, 0.1, 0.4 and 0.9. The plate-shaped and bulk samples have dimensions of ~ 6 × 6 × 0.7 mm^3 and ~ 5 × 6 × 7 mm^3, respectively. From each bulk, two 2 × 2 × 3 mm^3 pixels were cut and polished to study the timing performances of the tested materials. The pure BSO bulk was not cut in order to test its scintillation kinetics and Cherenkov yield as described in Section 2.6.

2.2. Transmission measurements

The transmission measurements of the samples tested were performed using a PerkinElmer LAMBDA 650 UV/VIS spectrometer. It is provided with a deuterium and halogen lamp and covers the wavelength range of 190 to 900 nm. The light source is split in two beams, one of which is focused on the tested sample. Both beams are then collimated through an optical system towards a PMT which measures their amount of light. By comparing the sample beam with and without the sample placed, the system is able to perform a transmission scan over the wavelength. The other one is used to monitor drifts of the whole system.

2.3. Light output measurements

The experimental setup employed to measure the light output of the BGSO samples consists of a Hamamatsu R2059 PMT connected to a DT5720 CAEN digitizer working in charge integration mode. An analog attenuator can be employed to avoid saturation of the signal. The whole setup is enclosed in a temperature controlled black box.

The excitation source employed was ^{137}Cs which emits 661.7 keV γ-rays. In order to maximize the light collection each sample was wrapped with Teflon and coupled to the PMT glass with glycerine (n = 1.47). Furthermore, in order to protect the PMT glass from external light, the PMT and the tested samples were covered with a light tight black paper lid.

Conversion to photons was obtained measuring the single photo-electron peak of the PMT and correcting for the quantum efficiency of the PMT convolved with the emission spectra of the samples.

2.4. Scintillation kinetics under pulsed X-ray excitation

The scintillation emission-time distribution of the samples tested was measured using a Time Correlated Single Photon Counting (TCSPC) [16] setup described in [17]. A pulsed diode laser (PicoQuant, PDL 800-B) is used as excitation source of an X-ray tube from Hamamatsu. It generates an X-ray beam with a continuous energy spectrum between 0 and 40 keV, with mean energy peak at 10 keV. The beam, after crossing a brass collimator, is directed towards the tested sample whereas the scintillation light is collected by a hybrid photomultiplier working in TCSPC mode. The measurements were done by hitting the sample with X-rays on one surface and detecting the emitted light from the same surface. The signal of the hybrid PMT reaches an amplifier and timing discriminator and is then used as the stop signal of a time to digital converter, while the start is provided by an external trigger of the pulsed diode laser. The impulse response function (IRF) of the setup is 180 ps FWHM.

In order to avoid air excitation to influence the emission-time distribution obtained, a band pass filter centred at 500 nm with 40 nm FWHM was placed in front of the hybrid PMT.

The scintillation emission-time profile was modelled as follows:

$$f(t) = \sum_{i=1}^{3} R_i \cdot \frac{\exp\left(-\frac{t-\theta}{\tau_{d,i}}\right) - \exp\left(-\frac{t-\theta}{\tau_r}\right)}{\tau_{d,i} - \tau_r} \cdot \Theta(t-\theta) + bkg \quad (1)$$

where $\tau_{d,i}$ is the ith component of the decay time constant, τ_r is the rise time constant, R_i is the weight of the ith component, θ is the instant above which the scintillation pulse starts and bkg is the background.

2.5. Coincidence time resolution setup

The coincidence time resolution (CTR) of the samples tested was measured using the setup described in [18,19]. In the setup two crystals coupled to SiPMs are facing each other and a ^{22}Na source is placed between them. The radioactive source emits two correlated 511 keV gammas back-to-back which are then detected by the scintillators. The SiPM signals are split into two branches: the first one is read out by high frequency electronics [18,20] for the time signal, while the other one is read out by an analog operational amplifier to extract the energy signal. Both these signals are then digitized by a LeCroy DDA735Zi oscilloscope. The data analysis is done offline with ROOT [21]. In order to evaluate the CTR, just the events within the photopeak have been taken into account. Furthermore a time-walk correction based on the measured signal rise time was performed in a similar fashion as discussed in [22,23]. This time-walk correction is able to account for fluctuations on the photon time density due to different numbers of detected Cherenkov photons for each event.

Each sample was wrapped with Teflon and glued with Cargille Meltmount optical glue (n = 1.58, cutoff at 300 nm) to the used SiPMs. Plate-shaped samples were coupled to a 6 × 6 mm^2 Broadcom SiPM biased at 38 V and measured in coincidence with a reference detector made of a 2 × 2 × 3 mm^3 BGO crystal coupled to a 3 × 3 mm^2 Broadcom SiPM. The measured coincidence time resolution of the whole system is a combination of the CTR of BGSO and the reference scintillator.

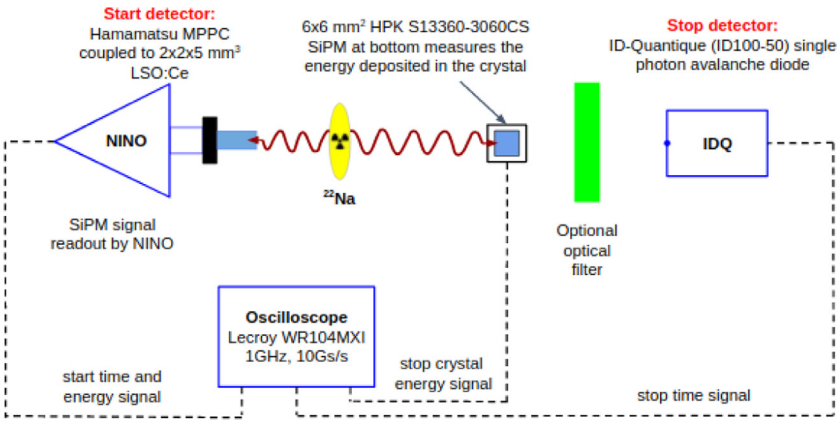

Fig. 1. Illustration of the TCSPC setup used to measure scintillation kinetics and Cherenkov yield of BSO. *Source:* The picture is based on a similar one from [24].

In order to evaluate the CTR of two identical plate-shaped samples (CTR_{sample}), the contribution due to the reference crystal (CTR_{ref}, which is 157 ± 3 ps FWHM and 352 ± 10 ps FWTM) has to be subtracted in quadrature from the measured value CTR_{meas} as shown in the following equation:

$$CTR_{sample} = \sqrt{2 \cdot CTR_{meas}^2 - CTR_{ref}^2} \tag{2}$$

Each $2 \times 2 \times 3$ mm^3 pixel was instead coupled to a 3.7×3.7 mm^2 Broadcom SiPM biased at 38 V and measured in coincidence with an identical one.

2.6. Scintillation kinetics and Cherenkov yield under 511 keV γ-excitation

In order to measure rise and decay times and the Cherenkov yield of the BSO bulk, a TCSPC setup [16] in which the only events selected are those in the 511 keV photopeak on both the start and stop detectors, was used. A detailed description of the setup shown in Fig. 1 is provided in [17,24]. The start detector consists of a $2 \times 2 \times 5$ mm^3 LSO:Ce codoped 0.4% crystal coupled to a Hamamatsu S13360-3050CS SiPM read out by a NINO chip [25]. As stop detector we used an ID-Quantique (IDQ) ID100-50 sensor, a single Geiger-mode avalanche photodiode with 50×50 μm^2 active area which reads out the light emitted from the BSO sample. A ^{22}Na source is placed between the start detector and the BSO bulk sample. The measurement was repeated placing a 500 nm bandpass filter (40 nm FWHM) from Thorlabs, which will be called "scintillation filter" in this paper, a second measurement with a Cherenkov filter also from Thorlabs which transmits light below 400 nm and above 670 nm, and one without any filter between the tested scintillator and the IDQ. The IRF of the whole setup was evaluated by placing a $2 \times 2 \times 5$ mm^3 PbF_2 crystal black painted on all sides except of the one facing the IDQ harvesting only Cherenkov photons. The IRF can be modelled with a Gaussian function having 122 ps FWHM. The transmission of the two filters used, as well as the measured photon detection probability (PDP) of the IDQ and scintillation and Cherenkov emission are plotted in Fig. 2, while Fig. 3 shows both BSO scintillation and Cherenkov spectra multiplied by the PDP of the IDQ and filters transmission as a function of the wavelength.

Considering the scintillation emission spectrum of the BSO sample defined by the function $\mathrm{Em}(\lambda)$, the Cherenkov spectrum $\mathrm{Ch}(\lambda) = A/\lambda^2$, the transmission of the filter $\mathrm{F}(\lambda)$ and the PDP of the ID-Quantique $\mathrm{PDP}(\lambda)$, it is possible to provide an analytical estimation of the expected ratio between the Cherenkov and scintillation yield as follows:

$$f = \frac{\int_{\lambda_{min}}^{\lambda_{max}} \mathrm{Ch}(\lambda)\ \mathrm{F}(\lambda)\ \mathrm{PDP}(\lambda)\ \mathrm{d}\lambda}{\int_{\lambda_{min}}^{\lambda_{max}} \mathrm{Em}(\lambda)\ \mathrm{F}(\lambda)\ \mathrm{PDP}(\lambda)\ \mathrm{d}\lambda} \tag{3}$$

where λ_{min} and λ_{max} define the range of wavelengths in which the optical photons generated in the BSO crystal are detected by the IDQ.

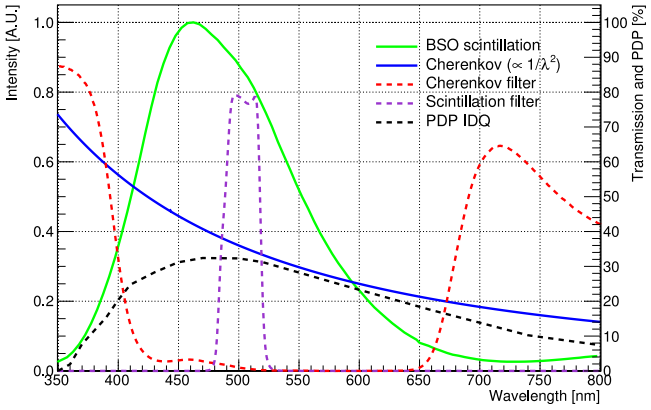

Fig. 2. BSO scintillation and Cherenkov spectrum, transmission of the filters tested as a function of the wavelength and PDP of the ID-Quantique.

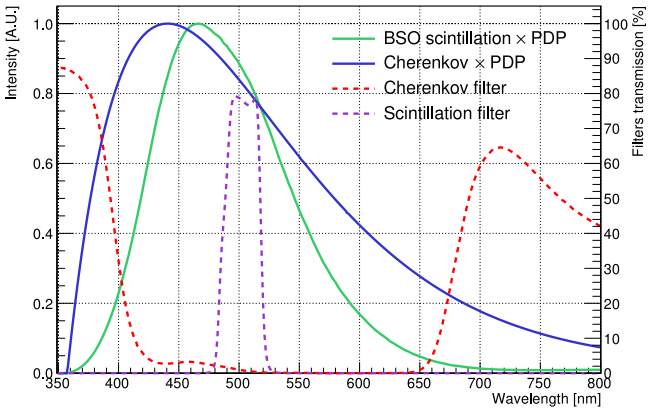

Fig. 3. BSO scintillation and Cherenkov spectrum multiplied by the PDP of the IDQ and transmission of the filters tested as a function of the wavelength.

3. Experimental results

3.1. Transmission measurements

The plot on the left side of Fig. 4 shows the transmission spectra of the plate-shaped samples. The results indicate that the transmission at higher wavelengths are similar for all the plate-shaped samples and they are transparent above ∼ 300 nm. Below this wavelength all samples gradually absorb light. From the left side of Fig. 4 it can be

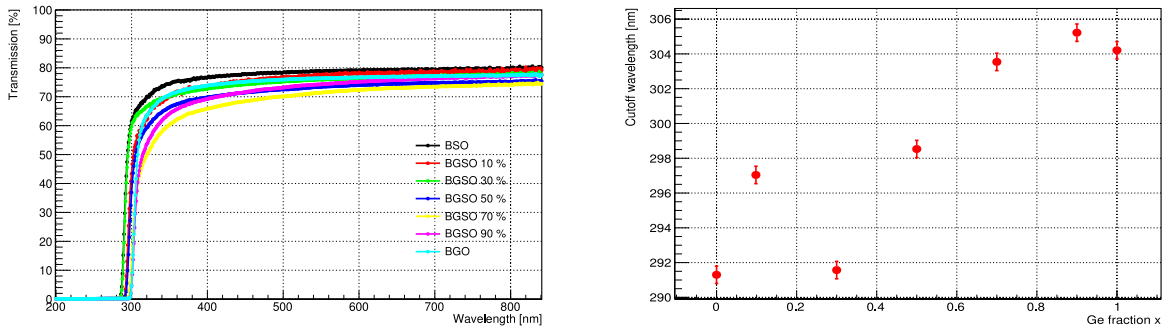

Fig. 4. Transmission spectra of the plate-shaped samples measured along their smallest dimension (left) and cutoff wavelength in transmission spectrum plotted against Ge fraction x (right).

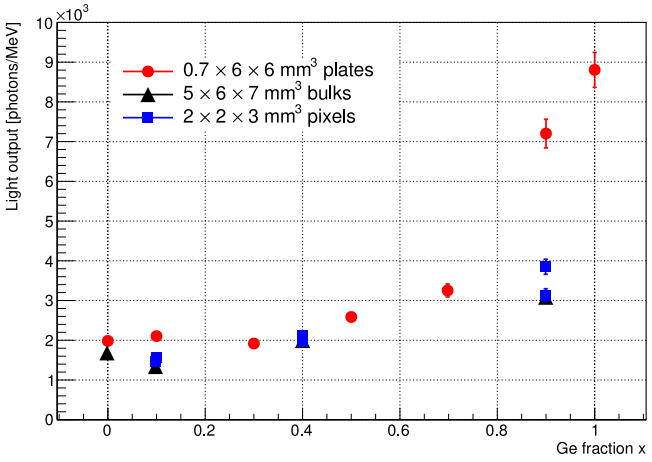

Fig. 5. Light output of the tested samples as a function of the Ge fraction x.

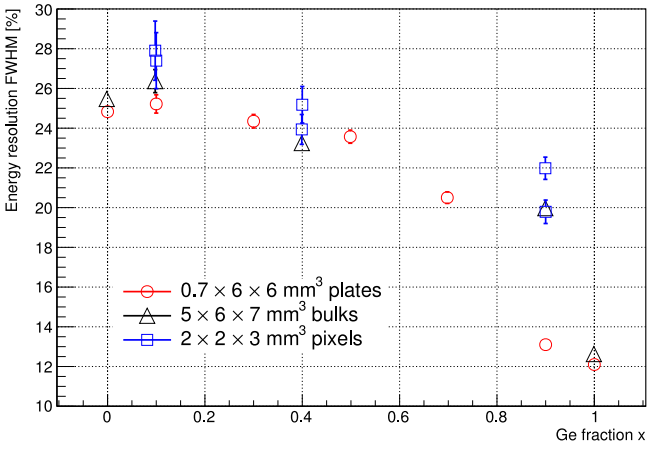

Fig. 6. Energy resolution of the tested samples as a function of the Ge fraction x.

observed that the cutoff wavelength below which the incident light is absorbed depends on the Ge fraction of the sample. The plot on the right side of Fig. 4 shows the cutoff wavelength, defined as the wavelength at which the transmittance is 40% of the value assumed in the stability region, as a function of the Ge fraction x. This plot indicates that the cutoff wavelength generally increases moving from BSO to BGO, except for the sample with $x = 0.1$, effect due to the worst surface condition.

3.2. Light output and energy resolution

The results achieved in terms of light and energy resolution are shown in Figs. 5 and 6 as a function of the Ge fraction x. The light output does not change significantly up to $x \simeq 0.3$ and then increases with the Ge fraction. Furthermore the light output of both pixels and bulk of BGSO 90% is much lower compared to the plate-shaped sample. This is due to impurities and internal defects of the tested sample as well as a lower light transmission efficiency for such kind of geometry.

The light output obtained for the BSO plate-shaped sample is about 22% of the BGO one, which is in agreement with literature [10].

In Fig. 7 the correlation between the energy resolution FWHM and the light output of the tested samples is presented and the points fitted with the following function:

$$ER = \frac{p_0}{\sqrt{LO}} \oplus p_1 \tag{4}$$

where p_0 and p_1 are parameters of the fit. The terms considered in this equation are related to photostatistics and intrinsic light output of the crystals respectively.

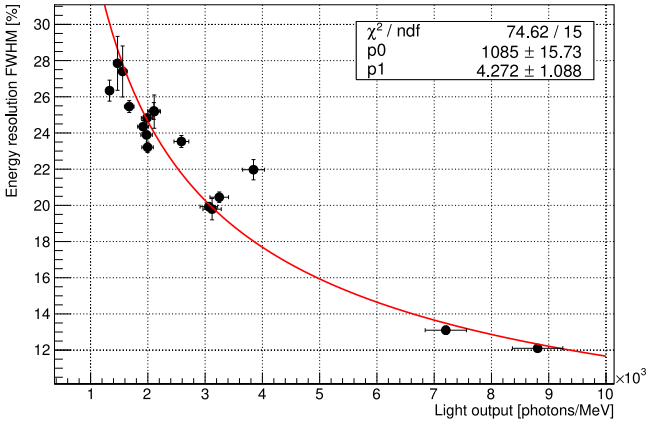

Fig. 7. Energy resolution FWHM plotted against the light output for each sample under test (plate-shaped, bulks and pixels).

3.3. Rise and decay time measurements

From the measurement performed with the X-ray TCSPC setup, emission-time distributions were obtained for each sample tested. An example of such distribution is shown in Fig. 8. The data have been fitted using a bi-exponential function having three decay time components and one rise time (see Eq. (1)).

The results achieved in terms of rise and decay times for all BGSO samples are summarized in Table 2. The scintillation rise times values of the plate-shaped samples are all below the resolution of the system ($\simeq$ 25 ps). The effective decay time is calculated as the weighted harmonic average $\tau_{d,eff} = \left(R_1/\tau_{d,1} + R_2/\tau_{d,2} + R_3/\tau_{d,3}\right)^{-1}$.

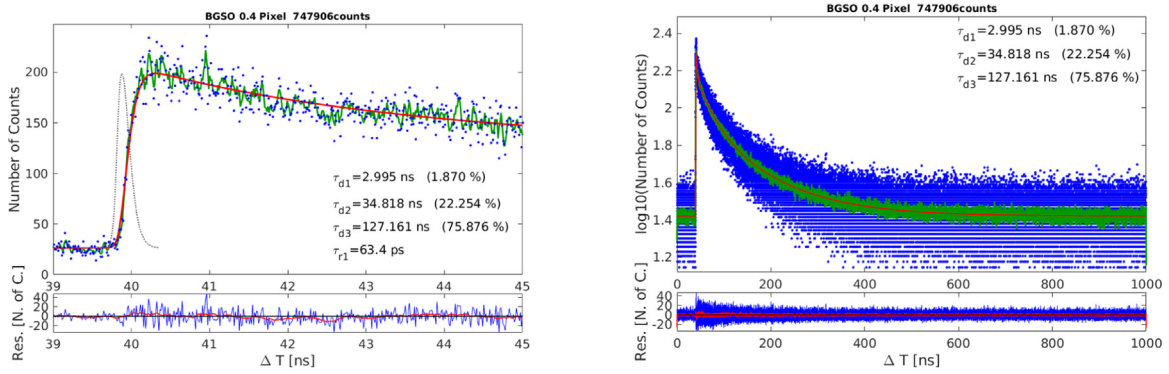

(a) Rising edge of the distribution (b) Falling edge of the distribution

Fig. 8. Time correlated single photon counting measurements exciting the BGSO 40% pixel with X-rays. The dotted line represents the impulse response function (IRF) of the setup, the green line is a sliding average with a window width of five bins of the distribution to guide the eye and the red solid line is the fit of the data.

Table 2
Parameters of the triple exponential used to fit the data from the measurements with the TCSPC setup for all the samples tested. τ_r is the rise time, $\tau_{d,i=1,2,3}$ are the decay time components and $R_{i=1,2,3}$ their corresponding abundances. An uncertainty of 10%, 6% and 2% can be assumed on the values of τ_{d1}, τ_{d2} and τ_{d3} extracted from the distributions respectively.

Plate-shaped samples (6 × 6 × 0.7 mm^3)							
Ge fraction	τ_{d1} (ns)	R_1	τ_{d2} (ns)	R_2	τ_{d3} (ns)	R_3	$\tau_{d,eff}$ (ns)
0	2.9	1.5%	27	9.7%	107	88.8%	58.6 ± 2.0
0.1	2.9	1.9%	34	23.6%	124	74.5%	51.3 ± 2.1
0.3	2.4	1.5%	24	13.1%	101	85.5%	49.9 ± 1.8
0.5	3.1	1.6%	33	19.3%	136	79.2%	59.4 ± 2.2
0.7	3.5	1.4%	37	15.4%	160	83.3%	75.1 ± 2.7
0.9	3.9	1.0%	45	9.5%	235	89.5%	117.1 ± 4.1
1	2.5	0.6%	47	8.0%	321	91.4%	144.5 ± 5.5

Pixels (2 × 2 × 3 mm^3)								
Ge fraction	τ_r (ps)	τ_{d1} (ns)	R_1	τ_{d2} (ns)	R_2	τ_{d3} (ns)	R_3	$\tau_{d,eff}$ (ns)
0.1	91	4.7	2.8%	42	25.1%	114	72.1%	54.9 ± 2.1
0.4	63	3.0	1.9%	35	22.3%	127	75.9%	53.8 ± 2.2
0.9	63	5.7	1.4%	52	11.6%	236	87.0%	118.3 ± 4.2

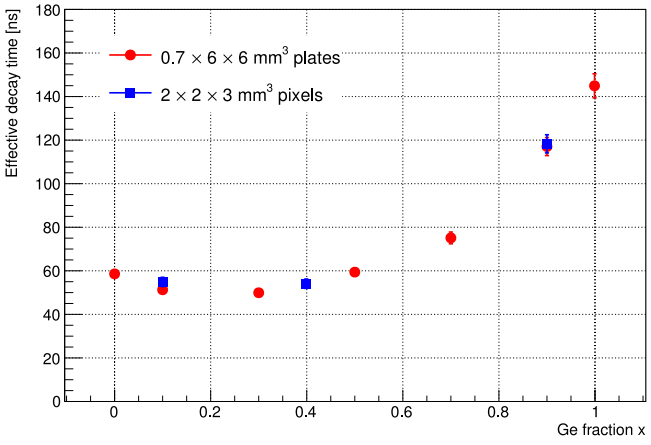

Fig. 9. Effective decay time of both plate-shaped samples and pixels as a function of the Ge fraction x.

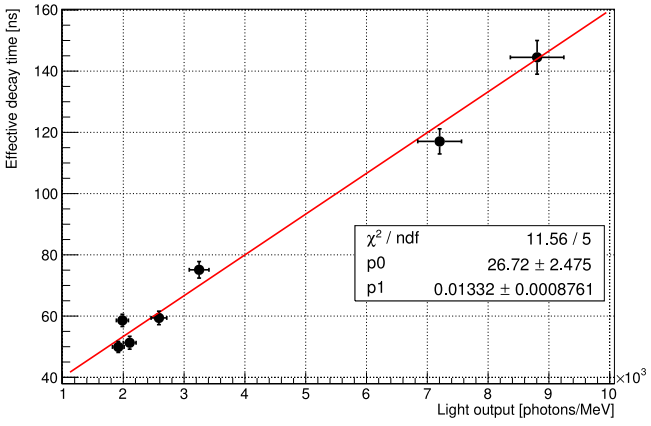

Fig. 10. Effective decay time of the plate-shaped samples as a function of their light output. The red solid line is a linear fit of the points.

The acceleration of the initial part of the decay region (approximated by the decay time components $\tau_{d,1}$ and $\tau_{d,2}$ in Table 2) is due to locally achieved high density of elementary excitations within the ionization track of the attenuated high energy photon [26]. The fact that the emission kinetics of these samples can be described using three decay time components is in agreement with literature [10,27].

The effective decay times achieved are also presented as a function of the Ge fraction x (see Fig. 9). An optimum effective decay time of 49.9 ± 1.8 ns is obtained for the $x = 0.3$ plate-shaped sample. A strong linear correlation between LY and decay time is observed as shown in Fig. 10.

3.4. CTR measurements

The CTR obtained from the measurements performed is extracted from delay distributions of the events with 511 keV deposition in both detectors similar to the one shown in the inset plot of Fig. 11 for the 40% Ge pixel. The distribution FWHM and FWTM are evaluated using a double-Gaussian fit. In Fig. 11 the CTR FWHM of the 40% Ge pixel is plotted against the leading edge threshold set on the oscilloscope. The points of each graph have been fitted using the following function $f(t \mid p_0, p_1, p_2) = \sqrt{p_0^2 + (p_1 \cdot t)^2 + (p_2/t)^2}$, where the dependency of the CTR from the threshold is related to both photostatistics (second term) and noise contribution (third term).

The CTR FWHM and FWTM values for each sample have been obtained by extracting the minimum from the fit function and are shown in Fig. 12. From these plots an optimum at $x \sim 0.5$ can be observed for both sets.

3.5. Scintillation kinetics and Cherenkov yield using 511 keV γ-excitation

The scintillation and Cherenkov photon emission-time distribution was measured with the TCSPC setup using 511 keV γ-excitation. Fig. 13 shows a zoom of the distributions obtained on the rising edge and

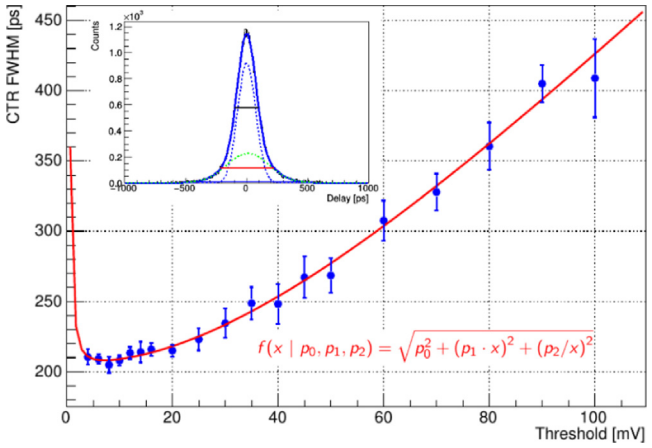

Fig. 11. CTR FWHM as a function of the oscilloscope threshold for the BGSO 40% pixels. The red solid line is the fit function. The delay distribution at 10 mV threshold is shown on the upper left side of the figure. The blue solid line is a double-Gaussian function which fits the distribution, the blue and green dotted lines are its components and the black and red horizontal lines provide the distribution FWHM and FWTM respectively.

Table 3
Summarizing table of the results achieved in terms of light output, energy resolution, effective decay time and CTR (FWHM and FWTM) for both sets of samples.

Plate-shaped samples ($6 \times 6 \times 0.7$ mm^3)					
Ge fraction	Light output (photons/MeV)	Energy resolution FWHM (%)	$\tau_{d,eff}$ (ns)	CTR FWHM (ps)	CTR FWTM (ps)
0	2000 ± 100	24.8 ± 0.2	58.6 ± 2.0	335 ± 10	970 ± 39
0.1	2100 ± 110	25.2 ± 0.5	51.3 ± 2.1	286 ± 8	682 ± 20
0.3	1900 ± 100	24.4 ± 0.3	49.9 ± 1.8	284 ± 12	692 ± 26
0.5	2600 ± 130	23.5 ± 0.3	59.4 ± 2.2	259 ± 8	651 ± 23
0.7	3200 ± 160	20.5 ± 0.3	75.1 ± 2.7	270 ± 10	685 ± 25
0.9	7200 ± 360	13.1 ± 0.2	117.1 ± 4.1	311 ± 9	747 ± 21
1	8800 ± 440	12.1 ± 0.2	144.5 ± 5.5	300 ± 12	756 ± 26
Pixels ($2 \times 2 \times 3$ mm^3)					
Ge fraction	Light output (photons/MeV)	Energy resolution FWHM (%)	$\tau_{d,eff}$ (ns)	CTR FWHM (ps)	CTR FWTM (ps)
0.1	1560 ± 80	27.4 ± 1.4	54.9 ± 2.1	217 ± 2	495 ± 9
	1470 ± 70	27.9 ± 1.5			
0.4	1980 ± 100	23.9 ± 0.8	53.8 ± 2.2	208 ± 2	441 ± 13
	2110 ± 110	25.2 ± 0.9			
0.9	3120 ± 160	19.8 ± 0.6	118.3 ± 4.2	244 ± 4	576 ± 20
	3850 ± 190	22.0 ± 0.6			

Cherenkov part applying the scintillation filter, the Cherenkov filter and without any filter. All the distributions have been normalized over the scintillation region without Cherenkov influence (between 106.5 ns and 200 ns) after background subtraction. A difference in Cherenkov peak height can be noticed in the three configurations examined. In particular, the Cherenkov filter suppresses a large fraction of scintillation, while the bandpass filter at 500 nm (scintillation filter) suppresses the UV part of Cherenkov light, as can be observed in Fig. 2.

This result demonstrates the possibility to efficiently separate Cherenkov light from scintillation emission using optical filters. Therefore the separation discussed above can be achieved using SiPMs having different spectral response which detect mostly scintillation light or Cherenkov photons.

Assuming the three plots perfectly overlapped over their pure scintillation region, it is possible to evaluate the ratio $f_{\text{filter}}/f_{\text{no filter}}$ between the fraction of Cherenkov light detected with and without filter placed. Such evaluation is performed after subtraction of the contribution due to scintillation from the Cherenkov peak height. The values obtained for such ratios from the distributions measured with the TCSPC setup are 3.1 ±0.6 and 0.7 ±0.1 for the Cherenkov and scintillation filters respectively. From the analytical calculation of these ratios starting from Eq. (3), the values obtained are $f_{\text{Cher}}/f_{\text{no filter}} = 3.19$ and $f_{\text{scint}}/f_{\text{no filter}} = 0.61$ in very good agreement with experimental results.

4. Discussion

In this work, several characterization measurements have been performed to understand the scintillation properties of mixed BGSO samples from two different producers. The most relevant results for the plate-shaped samples and the pixels are summarized in Table 3 showing that the results of the two sets are consistent.

The outcome of the transmission measurements of the plate-shaped samples shows that all the crystals are transparent above ∼ 300 nm and have similar transmission values at higher wavelengths. Small differences can be due to surface chips and cracks inside the samples. A feature which can be observed is the red-shift of the cutoff wavelength moving from BSO to BGO. A difference of about 13 nm was measured between pure BSO and BGO plate-shaped samples similarly to what reported in literature [8].

Light output measurements show a non-linear increase of the light output with the Ge fraction in the samples. As for the plate-shaped samples, the measured value is about 2000 photons/MeV up to 30% Ge fraction and than rapidly increases. The ratio between the light output of BSO and BGO plate-shaped samples is ∼ 22% and in line with literature [10].

The outcome of time correlated single photon counting measurements with X-ray excitation shows a dependence of the decay time components and abundances with the germanium fraction inside the sample. The evaluation of the effective decay time for each sample show that an optimum of 49.9 ± 1.8 ns is reached for the plate-shaped sample with 30% Ge and 53.8 ± 2.2 ns for the pixel sample with 40% Ge, while the one having the highest effective decay time is pure BGO.

As for coincidence time resolution measurements, it can be observed that some mixed BGSO samples have better timing compared to pure BGO and BSO for both sets. The optimum is reached around a Ge fraction $x = 0.5$ and is 259 ± 8 ps FWHM and 651 ± 23 ps FWTM for plate-shaped sample and 208 ± 2 psFWHM and 441 ± 13 ps FWTM for pixels. It is important to underline that, due to slightly different geometries and corner cracks of the plate-shaped samples analysed, the CTR values to be considered should be corrected to have a better understanding of the behaviour of the CTR variation with the Ge fraction. In particular, for what concerns the BSO sample, it was thicker (∼ 1 mm) compared to the other plates. Furthermore, the surface of this plate was slightly larger (∼ 6×7 mm^2), hence when coupled to a 6×6 mm^2 SiPM around 16% of the light is not detected yielding to an expected ∼ 8% deterioration in time resolution. Hence a CTR of 310 ±12 ps FWHM and 898 ± 36 ps FWTM is expected for this sample when having the same geometry as the other crystals.

Finally, the possibility to efficiently separate Cherenkov light by scintillation emission was demonstrated by means of a TCSPC setup with 511 keV γ excitation. The different filters employed in the measurements performed coupled to the ID-Quantique detector mimic the possible response of SiPMs sensitive to photons in different wavelength regions. Therefore this work shows the possibility to maximize Cherenkov light or scintillation emission detection using SiPMs which are sensitive to light emitted in a specific range of wavelengths.

5. Conclusions

The study performed on mixed BGSO samples has shown interesting features in terms of light output and timing which may make such kind of materials attractive in both high energy physics and medical imaging. In particular the measurements performed show better timing performances for mixed BGSO samples with 30%–50% of Ge fraction compared to pure materials. A coincidence time resolution at 511 keV

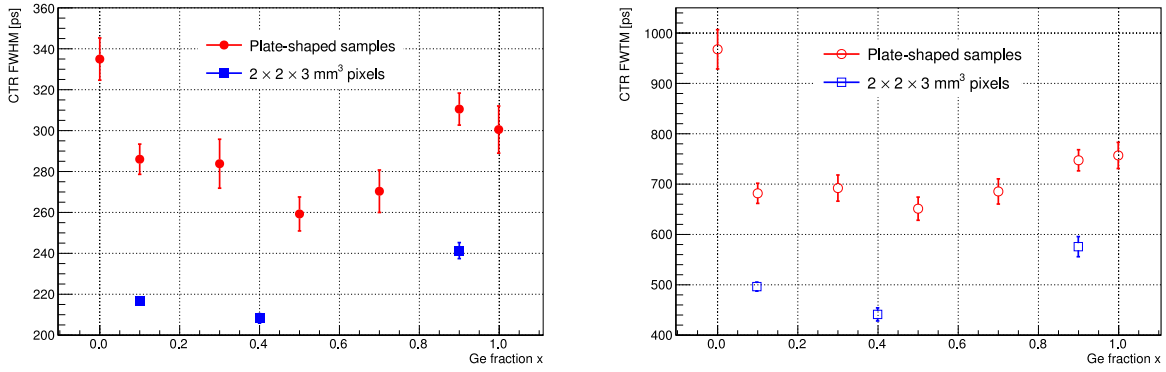

Fig. 12. CTR FWHM (left) and FWTM (right) of both the sets tested as a function of the Ge fraction x. A minimum at about $x = 0.5$ can be noticed for both sets.

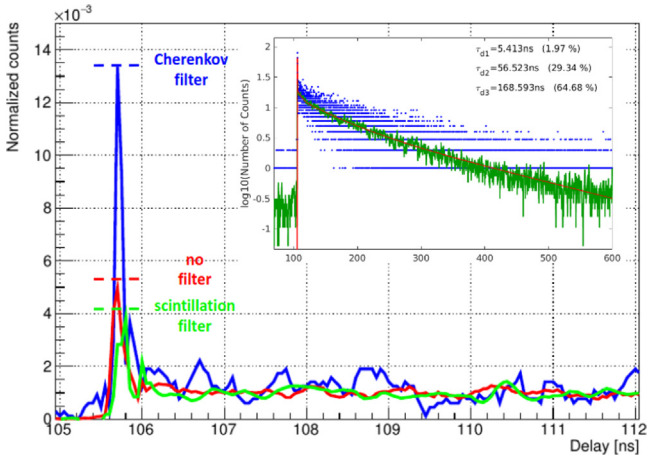

Fig. 13. Zoom on the rising edge and Cherenkov part of the TCSPC measurements of the BSO sample. On the upper right side the decay region of the signal produced by BSO without filter is shown.

of 208 ± 2 ps FWHM was measured for a 2 × 2 × 3 mm^3 BGSO pixel with 40% Ge fraction and an effective decay time of 49.9 ± 1.8 ns was achieved for a plate-shaped sample with 30% Ge fraction. Some samples measured also have a smaller slow decay time component (optimum of 101 ± 2 ns for a plate-shaped BGSO sample with 30% Ge fraction) compared to pure BGO and BSO which has a strong impact in reducing pile-up effects in high-rate environments. Therefore using mixed crystals is an effective strategy to tune the scintillating properties to a specific application.

Furthermore, Cherenkov and scintillation light produced in a pure BSO sample were efficiently separated using optical filters. The results obtained in this paper show that BSO or an optimized BGSO sample are leading candidates for dual-readout calorimetry with crystals at future e^+e^- colliders, given their faster decay time, lower scintillation and thus overall better chances to efficiently detect both Cherenkov and scintillation components.

CRediT authorship contribution statement

R. Cala': Conceptualization, Investigation, Software, Formal analysis, Validation, Writing – original draft. **N. Kratochwil:** Conceptualization, Investigation, Validation, Writing – review & editing. **L. Martinazzoli:** Conceptualization, Investigation, Software, Formal analysis, Validation, Writing – review & editing. **M.T. Lucchini:** Conceptualization, Writing – review & editing. **S. Gundacker:** Conceptualization, Software, Writing – review & editing. **E. Galenin:** Conceptualization, Samples preparation. **I. Gerasymov:** Conceptualization, Samples preparation. **O. Sidletskiy:** Conceptualization, Samples preparation, Writing – review & editing. **M. Nikl:** Conceptualization, Samples preparation, Writing – review & editing. **E. Auffray:** Conceptualization, Supervision, Resources, Writing – review & editing.

Declaration of competing interest

The authors declare that they have no known competing financial interests or personal relationships that could have appeared to influence the work reported in this paper.

Acknowledgements

This work was performed in the framework of the Crystal Clear Collaboration.

Partial support from Operational Programme Research, Development and Education financed by European Structural and Investment Funds and the Czech Ministry of Education, Youth and Sports (Project No. SOLID21 CZ.02.1.01/0.0/0.0/16_019/0000760) is acknowledged with thanks.

The authors are grateful to prof. Mitsuru Ishii from Shonan Institute of Technology for providing the set of BGSO crystals used in this study.

The authors thank Dominique Deyrail from CERN EP-CMX for thoroughly cutting and polishing of the BGSO bulk samples.

References

[1] L3 collaboration, B. Adeva, et al., The construction of the L3 experiment, Nucl. Instrum. Methods A 289 (1990) 35–102.
[2] P. Gianotti, on behalf of the PADME collaboration, The calorimeters of the PADME experiment, Nucl. Instrum. Methods A 936 (2019) 150–151.
[3] CMS collaboration, The CMS experiment at the CERN LHC, J. Instrum. 3 (2008) S08004.
[4] CMS collaboration, The CMS Electromagnetic Calorimeter Project: Technical Design Report, CERN-LHCC-97-33, 1997.
[5] R. Wigmans, Energy measurement at the TeV scale, New J. Phys. 10 (2008) 025003.
[6] A. Gola, et al., NUV-sensitive silicon photomultiplier technologies developed at foundazione Bruno Kessler, Sensors 19 (2019) 308.
[7] M.T. Lucchini, et al., New perspectives on segmented crystal calorimeters for future colliders, J. Instrum. 15 (2020) P11005.
[8] N. Akchurin, et al., A comparison of BGO and BSO crystals used in dual-readout mode, Nucl. Instrum. Methods A 640 (2011) 91–98.
[9] N. Akchurin, et al., Separation of crystal signals into scintillation and cherenkov components, Nucl. Instrum. Methods A 5995 (2008) 359.
[10] M. Ishii, et al., Development of BSO ($Bi_4Si_3O_{12}$) crystal for radiation detector, Opt. Mater. 19 (2002) 201–212.
[11] F. Yang, et al., BSO crystals for the HHCAL detector concept, J. Phys.: Conf. Ser. 587 (2015) 012064.
[12] F. Yang, et al., A study on radiation damage in BGO and PWO-II crystals, J. Phys.: Conf. Ser. 404 (2012) 012025.
[13] E. Galenin, et al., Engeeniring of mixed $Bi_4(Ge_xSi_{1-x})_3O_{12}$ scintillation crystals, Funct. Mater. (ISSN: 1027-5495) 22 (4) (2015) 423–428.
[14] P. Lecoq, et al., Inorganic scintillators for detector systems, in: Physical Principles and Crystal Engineering, second ed., Springer, Cham, 2017.

[15] The CMS Electromagnetic Calorimeter Group, Radiation hardness qualification of $PbWO_4$ scintillation crystals for the CMS Electromagnetic Calorimeter, J. Instrum. 5 (2010) P03010.
[16] L. Bollinger, G. Thomas, Measurement of the time dependence of scintillation intensity by a delayed-coincidence method, Rev. Sci. Instrum. 32 (1961) 1044–1050.
[17] S. Gundacker, et al., Precise rise and decay time measurements of inorganic scintillators by means of X-ray and 511 kev excitation, Nucl. Instrum. Methods A 891 (2018) 42–52.
[18] S. Gundacker, et al., High-frequency SiPM readout advances measured coincidence time resolution limits in TOF-PET, Phys. Med. Biol. 64 (2019) 055012.
[19] S. Gundacker, et al., Experimental time resolution limits of modern SiPMs and TOF-PET detectors exploring different scintillators and Cherenkov emission, Phys. Med. Biol. 65 (2020) 025001.
[20] J.W. Cates, et al., Improved single photon time resolution for analog SiPMs with front end readout that reduces influence of electronic noise, Phys. Med. Biol. 63 (2018) 185022.
[21] R. Brun, F. Rademakers, ROOT - An object oriented data analysis framework, Nucl. Instrum. Methods A 389 (1996) 81–86.
[22] N. Kratochwil, et al., Pushing Cherenkov PET with BGO via coincidence time resolution classification and correction, Phys. Med. Biol. 65 (2020) 115004.
[23] N. Kratochwil, et al., Exploring Cherenkov Emission of BGO for TOF-PET, IEEE, 2020.
[24] S. Gundacker, et al., Measurement of intrinsic rise times for various L(Y)SO and LuAG scintillators with a general study of prompt photons to achieve 10 ps in TOF-PET, Phys. Med. Biol. 61 (2016) 2802.
[25] F. Anghinolfi, et al., NINO: An ultrafast low-power front-end amplifier discriminator for the time-of-flight detector in the ALICE experiment, IEEE Trans. Nucl. Sci. 51 (2004) 1974.
[26] A. Gektin, A. Vasil'ev, Scintillator energy resolution and a way to improve it by kinetic waveform analysis, Radiat. Meas. 122 (2019) 108–114.
[27] S.E. Brunner, D.R. Schaart, BGO as a hybrid scintillator / Cherenkov radiator for cost-effective time-of-flight PET, Phys. Med. Biol. 62 (2017) 4421.